

# Electric Field Enhancement in Tip-Enhanced Raman Spectroscopy by Biocompatible Materials Coating on Substrate

F.S. KHADEMI AND M. BAHREINI\*

*School of Physics, Iran University of Science and Technology, Hengam st., 13114-16846, Tehran, Iran*

Received: 17.03.2024 & Accepted: 12.09.2024

Doi: [10.12693/APhysPolA.147.10](https://doi.org/10.12693/APhysPolA.147.10)

\*e-mail: [m\\_bahreini@iust.ac.ir](mailto:m_bahreini@iust.ac.ir)

In this article, tip-enhanced Raman spectroscopy is investigated as a precise method for the analysis of biological samples. Using the finite difference time domain, simulation is carried out to design the required structures for the study of these samples. At first, by comparing different tip-enhanced Raman spectroscopy structures and considering the material, dimensions, and other parameters in the simulation, the ideal structure is introduced from a physical point of view and considering the electric field enhancement. In the following, taking into account the effect of environmental and chemical reactions during testing on biological samples, biocompatible materials are used as substrate coating in the simulation. The impact of using these materials is investigated in comparison with the previous conditions. After performing the simulations, we concluded that Au, Cu, and Ag have the highest electric field enhancement, i.e., the presence of Au next to Cu and Au and Cu next to Ag leads to the enhancement of their electric field. In the following, we found that the material and thickness of the layer under the coating in the substrate and tip greatly influence the enhancement. Finally, we used five biocompatible materials as a coating when using the Au tip and substrate, which creates the greatest electric field enhancement. We saw that the use of biocompatible materials significantly reduces the enhancement, and the effects of the use of these five materials do not differ so much. In summary, using a 1 nm layer of biocompatible coating creates a much more favorable effect on enhancement than larger thicknesses.

topics: tip-enhanced Raman spectroscopy (TERS), electric field enhancement, finite difference time domain (FDTD), biocompatible

## 1. Introduction

Tip-enhanced Raman spectroscopy (TERS) is a combination of vibrational Raman spectroscopy and scanning probe microscopy (SPM). It has the chemical sensitivity of Raman spectroscopy and the nanometer spatial resolution of SPM microscopy. After the light hits the material, some phenomena, including absorption, transmission, or scattering, may occur. Each of these phenomena can provide basic information about the chemical structure of the material [1]. Raman spectroscopy was introduced in 1928, and it is a powerful method for chemical analysis and studying the molecular structure of solid, liquid, and gas materials [2, 3]. One of the main limitations of Raman spectroscopy is the weakness of the Raman signal. To overcome this defect, Fleishman et al. [4] introduced surface-enhanced scattering (SERS) in 1974. In this method, due to the use of a rough metal surface, enhancement of the electric field occurs, so the Raman signal is greatly enhanced [5]. The SERS method largely overcame the problem of the weak Raman

signal, but its spatial resolution remained at the same scale as Raman scattering (about 200 nm) [6]. To overcome this limitation, in 1985 Wessel [7] proposed that by combining the SERS technique and SPM microscopy, nanoparticles in TERS can be located or replaced with a sharp metal tip. By this method, the spatial resolution can be reduced to 10 nm [7]. In the TERS method, Raman signal enhancement occurs only near a sharp atomic tip, which is usually covered with metals such as Au or Ag and has a size in the range of 10 to 50 nm [8]. In this method, the metal tip is precisely set by the SPM microscope on the surface of the sample placed on the metal substrate. When the laser light with the appropriate wavelength is focused on the top of the tip, a strong electromagnetic field is created between the tip and the surface of the substrate. So, it enhances the Raman signal [6].

There are two enhancement mechanisms used to explain the enhancement phenomenon in the current study of tip-enhanced Raman scattering: chemical enhancement mechanism (CM) and electromagnetic field enhancement mechanism (EM). CM is similar to the resonance Raman enhancement effect

caused by the charge transfer between molecules and metals. EM is currently considered the main enhancement effect in TERS. When an external field laser of a specific frequency irradiates metal nanoparticles, the electromagnetic field around the surface of the metal nanoparticles will produce a strong enhancement effect. So, the Raman scattering signal of the molecules in the electric field is enhanced. This newly generated electromagnetic mode is the localized surface plasmon resonance (LSPR) [9]. In addition, the electric field enhancement of a pair of metal nanoparticles was calculated based on the Mie theory. It demonstrated that when the direction of the external radio field is added along the line of the two-particle centers, the enormous local electric field enhancement will be generated between the two nanoparticles [10]. This electromagnetic field enhancement makes the gap between the particles a “hot spot” for TERS [11]. When the molecule is around the gap position, its Raman scattering signal will be significantly enhanced [12].

The finite difference time domain (FDTD) is one of the most popular and widely applicable numerical methods for explicitly solving Maxwell’s equations. It gained popularity for a number of reasons, including the ability to solve up to  $10^9$  unknowns or more [13], robustness, and generality. With advancements in computer memory capacities, this large-memory but robust technique has gained an advantage over other numerical techniques, such as the discrete dipole approximation (DDA) [14], the finite element method (FEM) [15], and the rigorous coupled-wave analysis (RCWA) [16]. The advantages and disadvantages of each of these methods depend on many factors, including the need for multiple frequencies, the type of application, the volume of the required computational domain, etc. Due to limitations of the methods of moments (MoM or MM) procedure [15], a great interest in solutions of Maxwell’s equations arose in the early 90’s [13]. The FDTD technique was introduced by Yee in 1966. It has been developed to provide numerical solutions to Maxwell’s time-dependent curl equations in order to obtain modeling capabilities for a great variety of applications [13].

An arbitrarily shaped particle can be placed in a finite domain bounded by an absorbing boundary condition [17]. The electromagnetic properties of this particle and any host medium can be specified by assigning a permittivity, conductivity, and permeability at each grid point. The field components are calculated only at these points, and the space and time derivatives of the field components are approximated using finite difference expressions [18]. This method is very accurate and potent for simulations of tip-enhanced Raman spectroscopy. In 2009, Yang et al. [19] used three-dimensional finite difference time domain (3D-FDTD) simulations to investigate the field enhancement properties of TERS in order to find optimal geometric parameters of

the metal tip and the metal substrate under specific excitation wavelengths with side illumination. In 2012, Stadler et al. [20], using this method, investigated the electromagnetic (em) field in gap-mode TERS theoretically and experimentally for a range of commonly used and unusual metal and nonmetal substrates. In 2013, Kazemi-Zanjani et al. [21] used FDTD to precisely estimate the impact of both radially and linearly polarized sources on the enhancement of the electric field. In 2015, Meng et al. [22], in addition to optimizing the tip structural parameters, obtained an optimized configuration to guide the design and construction of an atomic force microscopy–tip-enhanced Raman spectroscopy (AFM-TERS) system with high efficiency. In 2021, Katebi Jahromi et al. [23] first used the 3D-FDTD technique to solve Maxwell’s equations in a limited computational range. By adjusting the cone geometry, they enhanced and evaluated precisely electric fields at the apexes of silver and gold tips. Then, in order to magnify the strength of the electric field at the tip, they proposed a grating structure to be implemented around the cone surface. By solving Maxwell’s equations corresponding to the proposed system, the magnitude of enhancement of the electric field intensity at the tip apex due to implementing grating has been evaluated [23].

In this research, using finite difference time domain simulation by Lumerical software, an attempt has been made to optimize the TERS technique for efficient measurements on biological samples. To perform most of the biomolecular experiments with the TERS method, a strong electrical field enhancement is needed. To provide this enhancement, metal tips and substrates are usually used. However, metals have poor biocompatibility, potentially introducing difficulties in characterizing native structure and conformation in biomolecules [24]. The hydrophobicity of metal surfaces leads to difficulty in deposition and can have a destructive effect on the structure of native protein or nucleic acid. For example, surface-enhanced Raman spectroscopy studies show that the plasmonic metal surface changes the nature of protein and DNA double-strand break [24]. To solve this problem, a thin layer of biocompatible materials is used as a substrate coating [25].

In this article, first, a comparison is made between the simulation of different structures used in biological experiments by means of the TERS method to achieve the appropriate electric field enhancement. According to the simulations carried out in this field, in order to prevent damage to the sample, the following biocompatible materials are used as a thin layer on metal substrates: muscovite mica [24], polyethylene [26], polystyrene [26], polyvinylpyrrolidone (PVP) [27], and poly(N-isopropylacrylamide) (PNIPAM) [27]. Their effect on enhancement in different modes is compared.

## 2. Simulation method

A finite difference time domain (FDTD) simulation was applied using Lumerical software. The geometry for simulation in this research is shown in Fig. 1. The tip is in the shape of a cone with a length of  $L$ , whose apex is a circle with a radius of  $r$ , and its end is a circle with a radius of  $D/2$ . It is located at a distance of  $d$  from the surface of the substrate with thickness  $t$ . Also, a linearly polarized light that makes an angle of  $\theta$  with the axis of the beam is applied to create Raman scattering [17, 28, 29].

It should be noted that in all TERS simulations, a tip with a length of 300 nm has been used. The tip is a circle with a radius of 25 nm and is located at a distance of 0.5 nm from the surface of the substrate with a thickness of 55 nm. Also, the cone angle of the tip was set to  $30^\circ$ . A plane wave is incident from the side at an angle of  $30^\circ$  on the nanocavity formed by the tip and substrate. The electric field amplitude was chosen to be 1.0 V/m. Perfectly matched layers (PML) boundary conditions were used on all boundaries for all simulations. To accurately simulate the tip–substrate distance, the Yee cell size was set to 0.4 nm. The nonuniform FDTD mesh method was used to save the computation resources and simulation time. A time-domain monitor was added to ensure the convergence of our calculations [19, 21–24].

### 2.1. Plasmonic enhancement

Plasmonic enhancement is one of the most remarkable phenomena associated with noble metals in the visible region. When light interacts with metals, collective oscillations of the conduction electrons, known as surface plasmons, can be excited at the metal surface. These excitations can lead to propagating waves on the surface (surface plasmon polaritons, SPPs) or localized resonances in nanomaterials (localized surface plasmon resonance, LSPR). SPPs propagate across a surface with momentum described by the following dispersion relation [30]

$$k_x = k_0 \sqrt{\frac{\varepsilon_1 \varepsilon_2}{\varepsilon_1 + \varepsilon_2}}, \quad (1)$$

where  $\varepsilon_1$  and  $\varepsilon_2$  are the permittivity of the two media at the interface,  $k_0 = \frac{\omega}{c}$  is the wavevector of the wave we seek in vacuum.

If surface plasmons are excited in subwavelength structures instead of interfaces, the result is a localized resonance that is non-propagating and can be used for strong field enhancements. The confinement of a surface plasmon happens in a metal nanostructure of size comparable to or smaller than the wavelength of light used to excite the plasmon, resulting in localized surface plasmons (LSPs).

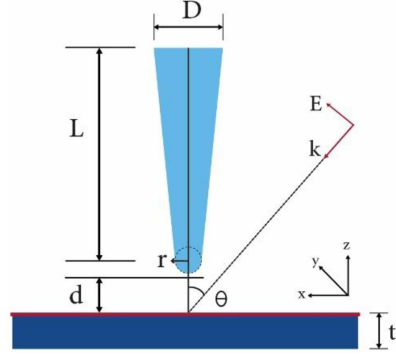


Fig. 1. The geometry of the tip, substrate, and electric field, and the parameters used in the simulation of tip-enhanced Raman spectroscopy.

When we consider the free electron model for metals where valence electrons are considered to be nearly free from the nuclei, damping is assumed to be caused by electrons scattering off of the nuclei. By including the contribution of damping, the electric permittivity  $\varepsilon(\omega)$  of the metallic material at the frequency angular  $\omega$  near the plasmon resonance  $\omega_p$ , the equation for the permittivity can be more accurately written as follows

$$\varepsilon(\omega) = \varepsilon_\infty - \frac{\omega_p^2}{\omega^2 - i\gamma\omega}. \quad (2)$$

Here,  $\omega_p$  is the plasma frequency of the free electron gas in the metallic material of the nanoparticles, and  $\gamma$  is the characteristic collision frequency in this electron gas, which signifies the amount of damping.

To show the enhancement of the em field in the free space surrounding metallic nanoparticles due to the effect of their LSPR, we start by considering one metallic spherical nanoparticle with radius  $\rho$ . We denote it by  $\varepsilon(\omega)$  — the effective dielectric constant or electric permittivity of the metallic material with respect to the electrical field in the monochromatic electromagnetic radiation with the angular frequency  $\omega$ . Electrical dipole moment  $p(R, t)$  inside the metallic spherical nanoparticle with the center located at some point of  $R$  in the space is  $p(R, t) = 4\pi\varepsilon_m\rho^3 L(\omega)E^{(0)}(R, t)$ , where the local field can be expressed as

$$L(\omega) = \frac{\varepsilon(\omega) - \varepsilon_\omega}{\varepsilon(\omega) + 2\varepsilon_m}. \quad (3)$$

If  $\varepsilon(\omega) = 2\varepsilon_m$ , the denominator is zero, which makes the local field  $L$  infinite. This can only happen if the dielectric function is negative, i.e., the frequency is less than the plasma frequency [30].

As a result, local electric fields within the metal nanostructures can achieve strengths with orders of magnitude higher than that of the incident field. This enhanced electromagnetic field has a wide variety of applications, such as surface-enhanced spectroscopies [31], non-linear optics [32], and near-field nanoablation with plasmonic nanoparticles

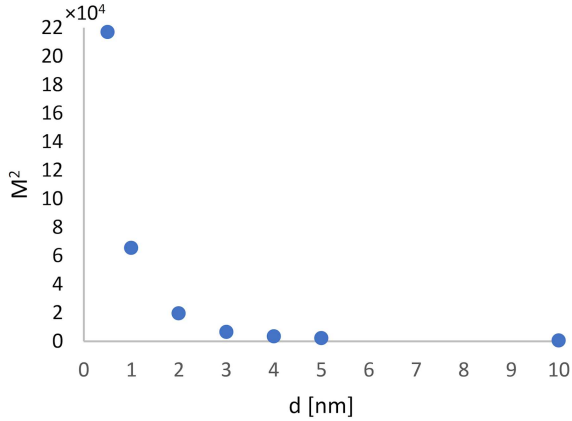


Fig. 2. Electric field enhancement at different distances between the tip and the substrate using the Au tip and substrate in tip-enhanced Raman spectroscopy.

called plasmon-assisted ablation. The best-known techniques based on plasmonic enhancement are surface-enhanced Raman scattering (SERS) and TERS.

## 2.2. TERS enhancement factor

When the optical fields present on metal nanostructures are induced by an incident wave, the field enhancement factor  $EF$  can be described as the ratio of the local electric field to that of the incident electric field. Since light intensity depends on the square of the em field strength, the intensity of the enhanced light field at the laser wavelength scales as the power of the enhancement factor of the em field at laser wavelength as  $EF_{\text{Laser}}^2$ . The Raman scattered light is also enhanced in a TERS experiment, expressed as  $EF_{\text{Raman}}^2$ . In a short spectral range close to the laser wavelength, the enhancement factor of the Raman signal is at the same scale as the em field enhancement factor at the laser wavelength  $EF_{\text{Field}}^2$ . Thus, the enhancement factor of the TERS signal can be approximated as [1, 33]

$$EF_{\text{TERS}} = EF_{\text{Laser}}^2 EF_{\text{Raman}}^2 \approx EF_{\text{Field}}^4 = M^4, \quad (4)$$

where  $M = |E_{\text{tip}}|/|E_0|$ .

In TERS experiments, the TERS enhancement factor  $EF_{\text{TERS}}$  for a surface with uniform molecular coverage is determined from the measured near- and far-field optical intensities of  $I_{\text{NF}}$  and  $I_{\text{FF}}$ , respectively, the size of the far-field focus  $A_{\text{FF}}$ , and the spatial extent of the tip-enhanced region  $A_{\text{NF}}$ . The equation that is used to determine the experimental value of the TERS enhancement factor is written as [33]

$$EF_{\text{TERS}} = \frac{I_{\text{NF}}}{I_{\text{FF}}} \frac{A_{\text{FF}}}{A_{\text{NF}}}. \quad (5)$$

## 3. Results and discussion

When reviewing the articles related to TERS experiments in biological fields, it can be seen that Au, Ag, and Cu are usually used as the tip and substrate to achieve high electrical enhancement. These metals have some advantages and disadvantages. In short, all three metals offer a favorable electric field enhancement, however, using these materials is associated with challenges such as the high cost of Au, the rapid oxidation of Ag exposed to air, and the high reactivity of Cu, as a result of its low chemical stability [20, 27, 29, 34, 35].

At the beginning of our study, the effect of increasing the distance between the tip and the substrate on the enhancement of the electric field will be investigated, so the appropriate distance used in the simulations will be selected. Also, due to the fact that TERS experiments usually use Si tips coated with various metals [36], the effect of using Si in the bottom layer of the tip will be investigated in the simulation. In the following, the simulations of different states of use of Au, Ag, and Cu will be examined. At first, by using the tip and substrate with the same material, the electric field enhancement will be numerically compared with each other. Then, in order to increase the electric field enhancement and reduce the reactivity of the surfaces by using different types of coatings for the tip and the substrate, the effect of using each layer in each simulation should be determined numerically. In the end, in order to prevent damage to the sample, biocompatible materials are used as a thin layer on metal substrates. Their effect on strengthening in different states is also compared.

### 3.1. The effect of distance between tip and substrate

In this simulation, the Au tip and substrate are used at different distances from each other. A laser with a wavelength of 633 nm is used. According to Fig. 2, when the distance between the tip and the substrate increases between 0.5 and 3 nm, the electric field enhancement decreases with a large slope. Above the distance of 3 nm, until the substrate is placed at an infinite distance from the tip, or in other words, when the tip is used without the presence of the substrate, the electric field enhancement decreases with a very small slope. Also, it can be seen that among the enhancements dependent on the location of the tip, the highest enhancement is at the wavelength of 633 nm at the distance of 0.5 and 1 nm. At distances greater than 2 nm, the lowest electric field enhancement is created at the apex of the tip. Therefore, it is suggested that a higher enhancement at the tip apex be created. The tip and the substrate should be placed at a distance of 0.5 or, most, 1 nm from each other.

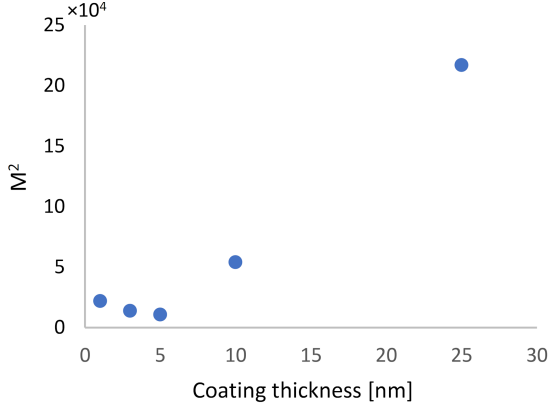


Fig. 3. Electric field enhancement at different thicknesses of the Au coating on the Si tip using the Au substrate in tip-enhanced Raman spectroscopy.

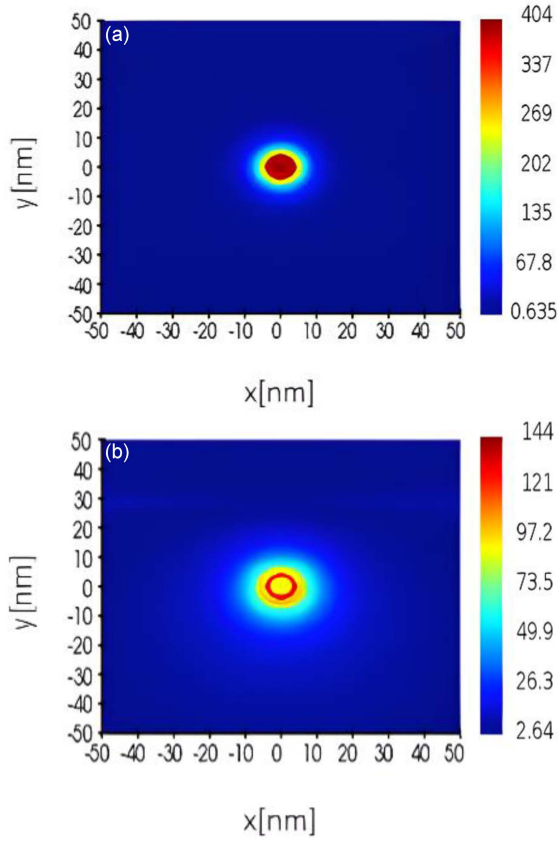


Fig. 4. Electric field distribution along the  $z$ -axis in the case of (a) using Au tip and substrate and (b) using Si tip with 1 nm Au coating and Au substrate at a distance of 0.5 nm between the tip and the substrate and a wavelength of 633 nm in tip-enhanced Raman spectroscopy.

It should be noted that in some experimental articles, the sample is also considered in the simulations according to the specific materials used for analysis [37, 38]. Although a sample layer between the tip and the substrate affects the results, this research does not consider it. We did not examine a specific

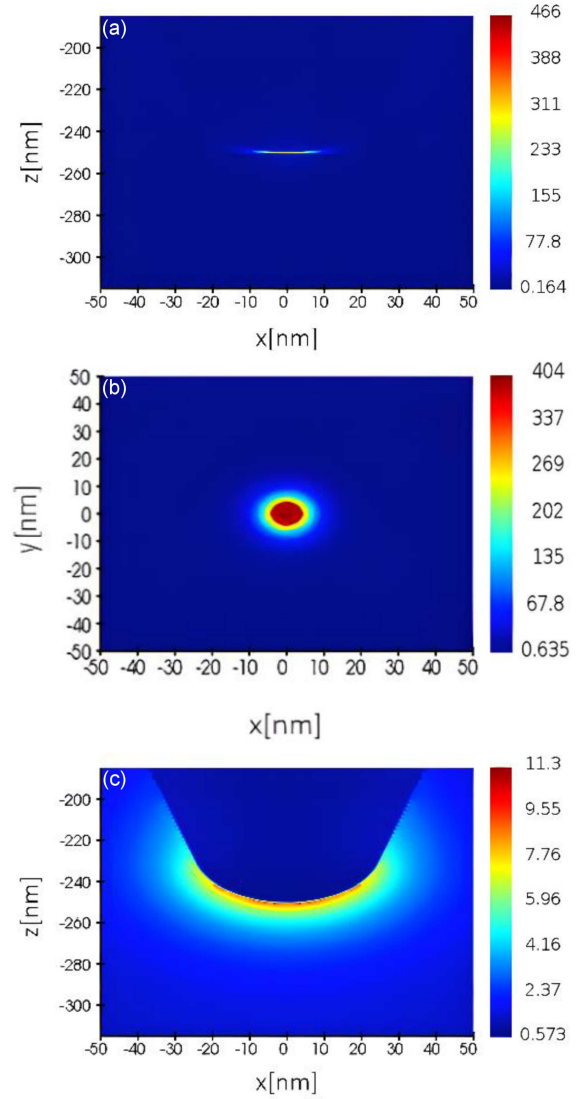


Fig. 5. Distribution of the electric field in the case of (a) using the Au tip and substrate along the  $y$ -axis at a distance of 0.5 nm from each other and a wavelength of 633 nm, (b) state (a) along the  $z$ -axis, (c) state (a) without considering the substrate in tip-enhanced Raman spectroscopy.

sample because the variety of biological materials has different refractive indices. We just considered the general state. However, in future research, we could focus on one specific biological sample and its effects on the electric field enhancement.

### 3.2. The effects of using Si tip with Au coating in different thicknesses

In the experimental tests of the TERS method, Si tips with the metal coating are usually used. In this section, the use of Si tip with different thicknesses of Au coating and the use of pure Au tip

TABLE I

Comparison of the electric field enhancement ( $|M|^2$ ) and the  $y$  component of the electric field ( $|M|$ ) in terms of wavelength for the modes of using the tip and substrate with different combinations of Au, Cu, and Ag.

Type	$\lambda$ [nm]	$ M $	$ M ^2$
Au tip and Ag substrate	532	156	24336
	633	393	154449
	785	175	30625
Au tip and Cu substrate	532	139	19321
	633	430	184900
	785	181	32761
Ag tip and Au substrate	532	250	62500
	633	398	158404
	785	178	31684
Ag tip and Cu substrate	532	280	78400
	633	360	129600
	785	179	32041
Cu tip and Au substrate	532	169	28561
	633	426	181476
	785	179	32041
Cu tip and Ag substrate	532	204	41616
	633	349	121801
	785	175	30625

are compared. In all these simulations, the tip radius is considered to be 25 nm. As can be seen in Fig. 3, the enhancement decreases with increasing thickness from 1 to 5 nm. This means that a 1 nm thickness provides better enhancement than a 5 nm thickness. From the thickness of 5 to 25 nm, the enhancement rises and reaches its maximum value in the case of using a pure Au tip.

Figure 4 shows the electric field distribution along the  $z$ -axis in two cases: using an Au tip and a Si tip with 1 nm Au coating. The substrate has a thickness of 55 nm. The Au substrate is located at a distance of 0.5 nm from the tip. It should be noted that in this research, the tip coating is assumed ideally as a constant layer, as in some other simulation articles [21, 22, 37]. However, it is hard to achieve such homogeneous and continuous coating experimentally.

### 3.3. The effects of using the tip and substrate in three cases with the same material

In this part, the electric field enhancement is investigated in three cases using the tip and substrate with the same material — Au, Ag, or Cu. The simulation of the Au tip and substrate can be seen in Fig. 5. According to Fig. 6, the maximum

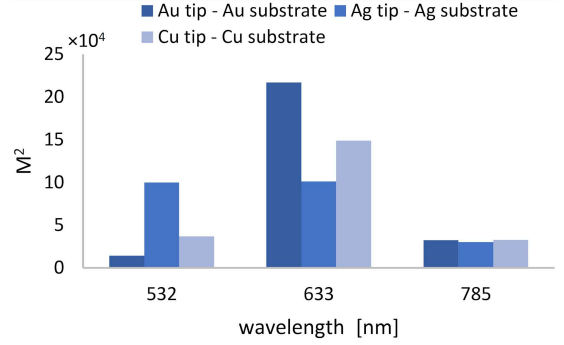


Fig. 6. Comparison of electric field enhancement in terms of wavelength for the use of Au, Ag, and Cu tips and substrates with a distance of 0.5 nm in tip-enhanced Raman spectroscopy.

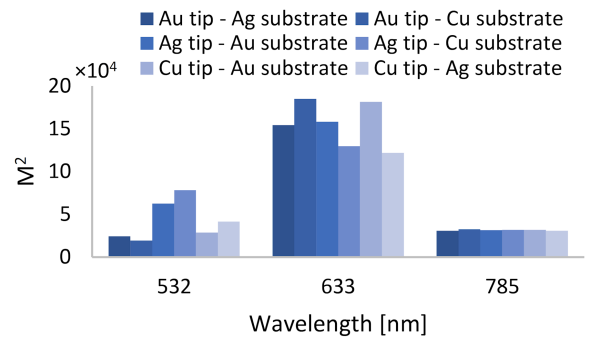


Fig. 7. Comparison of the electric field enhancement at three wavelengths for the use of tip and substrate at a distance of 0.5 nm with different materials — Au, Cu, and Ag — in tip-enhanced Raman spectroscopy.

enhancement of the electric field for the tips and substrates of Au, Cu, and Ag is at a wavelength of 633 nm. At a wavelength of 785 nm, all three structures show almost the same reaction. At a wavelength of 532 nm, a higher enhancement can be obtained by using Ag. Au and Ag have favorable effect on electric field enhancement due to their high free electron density. However, Cu and Au have favorable effect due to their low extinction coefficient (the imaginary part of the dielectric constant). Having a high extinction coefficient, Ag absorbs a large share of incoming light compared to Au and Cu, thereby reducing the electric field enhancement [34, 39, 40].

### 3.4. The effects of using different metals for the tip and substrate

The maximum enhancement of the electric field is obtained by comparing the different modes of using different metals for the tip and the substrate, as can be seen in Table I and Fig. 7, at

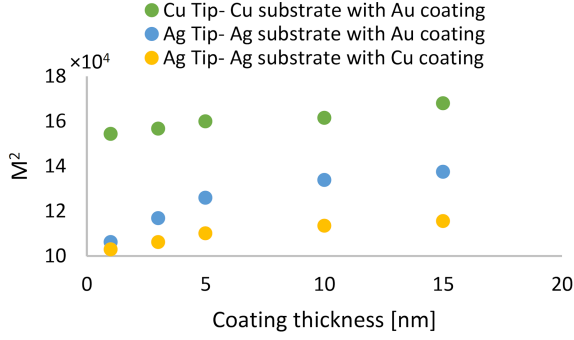


Fig. 8. The comparison of the electric field enhancement in terms of using the different thicknesses of Au and Cu substrate coating for Cu and Ag tips and substrates in tip-enhanced Raman spectroscopy.

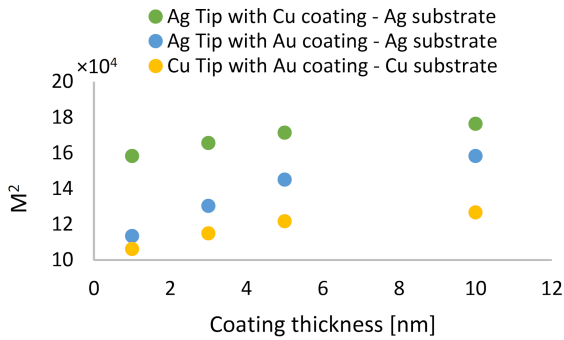


Fig. 9. Comparison of the electric field enhancement of different thicknesses of Au and Cu tip coating for Cu and Ag tips and substrates in tip-enhanced Raman spectroscopy.

a wavelength of 633 nm. In each case, at the wavelength of 785 nm, the materials of the tip and the substrate do not have a special effect on enhancement. At the wavelength of 532 nm, better enhancement is created when Ag is used, especially as a tip. In the case of using Au tip and substrate, the maximum electrical enhancement can be obtained. The combination of Au with Ag and Cu will not increase the enhancement. When using a Cu tip or substrate, using Au next to it increases, and using Ag decreases the enhancement of the electric field. Finally, when using an Ag tip or substrate, Au or Cu next to Ag increases its electric field.

### 3.5. The effects of using Au and Cu metal coating on the tip and substrate with Cu and Ag materials

According to Fig. 8, the use of Au coating for the Ag substrate has a greater effect on the increase in enhancement than the other two cases of using the coating on the substrate. However, the Au coating next to the Cu substrate creates a stronger electric field enhancement.

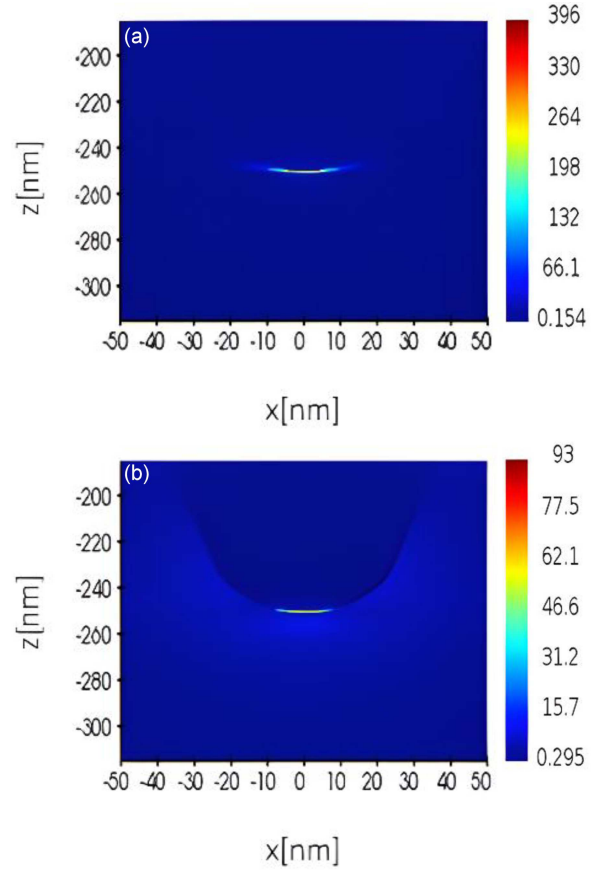


Fig. 10. The distribution of the  $y$  component of the electric field at a distance of 0.5 nm between the tip and the substrate at a wavelength of 633 nm in tip-enhanced Raman spectroscopy. It was done in two cases: (a) using a Cu substrate with 3 nm Au coating and Cu tip and (b) using glass ( $SiO_2$ ) instead of the Cu substrate in case (a).

According to Fig. 9, the use of an Au cover for the Ag tip has a greater effect on increasing the enhancement than in the other two cases when the coating for the tip is used. However, the Au coating next to the Cu tip creates a greater electric field enhancement.

### 3.6. Investigating the underlying layer in the substrate using glass

In this section, we will examine the effect of the underlying layer in the simulations. The purpose is to find out if the increase in electric field enhancement is more related to the coating itself or the interaction between the coating and the underlying layer when using different coatings. In Fig. 10, it can be seen that the material of the bottom layer of the substrate has a great effect on the enhancement of the electric field when using glass instead of Cu in the bottom layer.

TABLE II

Electric field enhancement of different coating thicknesses of biocompatible materials on the Au substrate using the Au tip at a distance of 0.5 nm between the tip and the substrate and a wavelength of 633 nm in tip-enhanced Raman spectroscopy.

Substrate coating	Index of refraction	Thickness [nm]	1	3	5	10
muscovite mica	$n = 1.6$	$ M $	282	125	97.5	65.1
	$k = 0$	$ M ^2$	79524	15625	9506.25	4238.01
PNIPAM	$n = 1.5012$	$ M $	266	137	87.5	57.4
	$k = 0.0022$	$ M ^2$	70756	18769	7656.25	3294.76
polyethylene	$n = 1.519$	$ M $	269	139	89.3	58.7
	$k = 0.002$	$ M ^2$	72361	19321	7974.49	3445.69
polystyrene	$n = 1.5875$	$ M $	280	149	96.3	64.2
	$k = 0$	$ M ^2$	78400	22201	9273.69	4121.64
PVP	$n = 1.5252$	$ M $	27	140	89.9	59.2
	$k = 0.0018$	$ M ^2$	729000	19600	8082.01	3504.64

### 3.7. The effects of using different thicknesses of Cu substrate

In this part, different thicknesses of Cu have been used as the bottom layer of the substrate. The aim is to check whether the increase in the electric field enhancement is only due to the use of the coating or due to the interaction between the coating and the substrate when using the Au coating on the substrate. According to Fig. 11, in the case of thicknesses of 15 to 35 nm of Cu, the enhancement increases with a large slope. However, in the case of thicknesses of 35 to 55 nm, the enhancement of the electric field decreases with a very small slope.

### 3.8. Effects of using biocompatible materials as a substrate coating

A strong field enhancement is needed to perform most of the biomolecular experiments with the TERS method. To provide this enhancement, metal tips and substrates are usually used. However, metal surfaces are generally not biocompatible. To solve this problem, a thin layer of biocompatible materials can be used as a substrate coating [24]. There may be a concern that the use of biocompatible materials will interfere with the TERS signal. However, it should be mentioned that the effectiveness of using, for example, PVP and muscovite mica as biocompatible coatings was confirmed in the surface-enhanced Raman scattering in living cells experiment and in tip-enhanced Raman spectroscopy for DNA experiment [24, 41].

In this section, as can be seen in Table II, five biocompatible materials are used as substrate coating with different thicknesses in the case of using Au tip and Au substrate. These biocompatible materials include muscovite mica, polyethylene (PE),

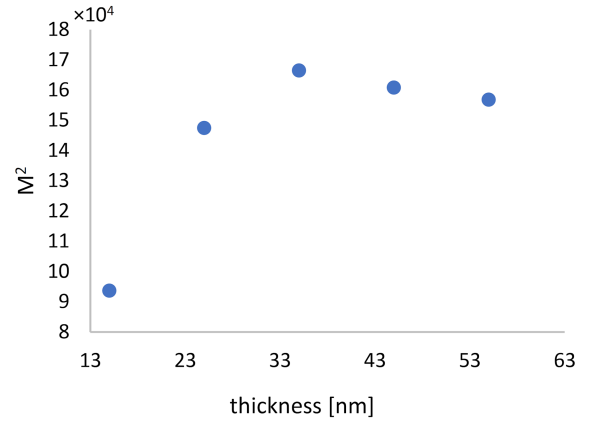


Fig. 11. The electric field enhancement of different thicknesses of the Cu substrate in the case of Cu substrate with 3 nm Au coating and Cu tip, at a distance of 0.5 nm between the tip and the substrate and a wavelength of 633 nm in tip-enhanced Raman spectroscopy.

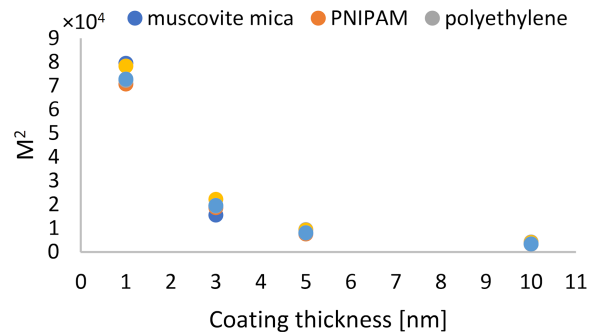


Fig. 12. Electric field enhancement of different coating thicknesses of biocompatible materials on the Au substrate using the Au tip at a distance of 0.5 nm between the tip and the substrate and a wavelength of 633 nm in tip-enhanced Raman spectroscopy.

TABLE III

The summary of electric field enhancement results: different simulation states of tip-enhanced Raman spectroscopy.

State		$ M ^2$		State	$ M ^2$
1	Au tip and Au substrate with 0.5 nm distance	217156	15	Cu tip and Ag substrate	121801
2	Au tip and Au substrate with 1 nm distance	65536	16	Ag tip and Au substrate	158404
3	Au tip and Au substrate with 1 nm mica coating	79524	17	Ag tip and Cu substrate	129600
4	Au tip and Au substrate with 3 nm mica coating	15625	18	Cu tip and Cu substrate with 3 nm Au coating	156816
5	Au tip and Au substrate with 10 nm mica coating	4238.01	19	Ag tip and Ag substrate with 3 nm Au coating	116964
6	Si tip with 1 nm Au coating and Au substrate	22201	20	Ag tip and Ag substrate with 3 nm Cu coating	106276
7	Si tip with 5 nm Au coating and Au substrate	11025	21	Cu tip with 3 nm Au coating and Cu substrate	165642
8	Si tip with 10 nm Au coating and Au substrate	54289	22	Ag tip with 3 nm Au coating and Ag substrate	130321
9	Au tip and Au substrate	217156	23	Ag tip with 3 nm Cu coating and Ag substrate	114921
10	Cu tip and Cu substrate	148000	24	Cu tip and Cu substrate with 3 nm Au coating	156816
11	Ag tip and Ag substrate	101000	25	Cu tip and SiO <sub>2</sub> substrate with 3 nm Au coating	8649
12	Au tip and Cu substrate	184900	26	Cu tip and 15 nm Cu substrate with 3 nm Au coating	93636
13	Au tip and Ag substrate	154449	27	Cu tip and 35 nm Cu substrate with 3 nm Au coating	166464
14	Cu tip and Au substrate	181476	28	Cu tip and 55 nm Cu substrate with 3 nm Au coating	156816

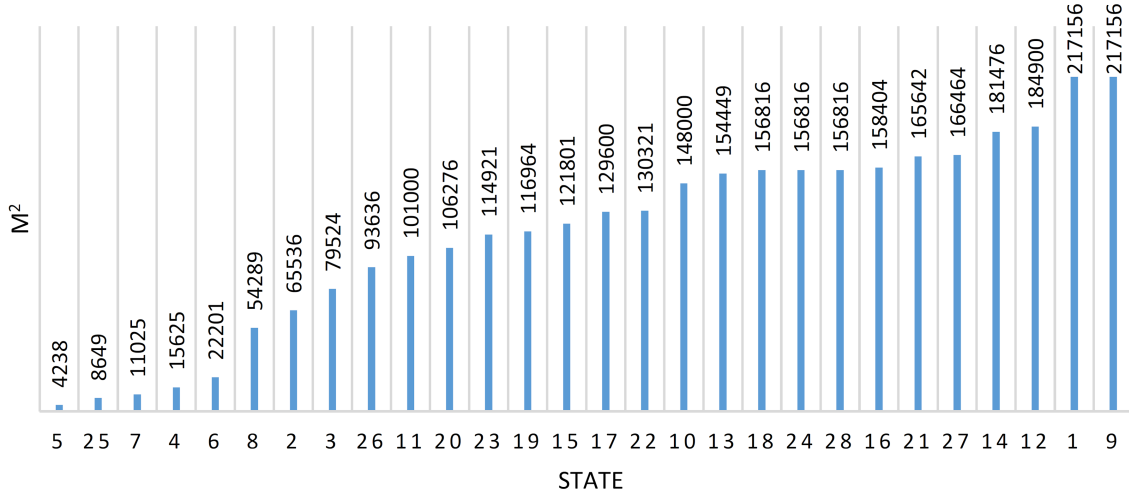


Fig. 13. The comparison of electric field enhancement results of different simulation states of tip-enhanced Raman spectroscopy.

PNIPAM, polystyrene, and polyvinyl pyrrolidone (PVP). The electric field in the  $y$ -axis is 466 (see Fig. 5a). The materials used in this simulation are defined in the software according to the refractive index (real part ( $n$ ) and imaginary part ( $k$ )) at the

wavelength of 633 nm. According to the results, muscovite mica, polystyrene, PVP, polyethylene, and PNIPAM provide higher enhancement. However, the improvements with these five materials are slightly different. Also, according to Fig. 12, the

electric field enhancement decreases strongly with a large slope when using 1 to 3 nm of the coating for the substrate. However, in thicknesses greater than 4 nm, the enhancement becomes almost constant. The electric field component is reduced from 466 to 282 in the best case, i.e., it is virtually halved and faces a significant reduction. However, according to the cases reviewed in Table II, the use of a 1 nm layer of biocompatible coating creates a much more favorable effect on enhancement than other modes.

### 3.9. In summary

A comparison between the electric field enhancement presented in Sects. 3.1 to 3.8 has been made in this section, as can be seen in Table III and Fig. 13. Because the highest electric field enhancement was observed in all cases at the wavelength of 633 nm, in this section only the enhancement of different states at this wavelength is compared. Due to the greater enhancement that mica offers compared to other materials, only this material has been examined for comparison in three different thicknesses of biocompatible materials. In all TERS simulations, a tip with a length of 300 nm, whose top is a circle with a radius of 25 nm and a substrate with a thickness of 55 nm, have been used.

## 4. Conclusions

In this article, at first, the effect of increasing the distance between the tip and the substrate on the enhancement of the electric field was investigated. It was suggested that the tip and the substrate should be placed at a distance of 0.5 or at most 1 nm from each other to create a higher enhancement at the top of the tip.

In the next simulation, the difference of using a Si tip with different thicknesses of Au coating was investigated in comparison with the case of using a fully Au tip, taking into account the fact that in the experimental TERS method, Si tips with metal coatings are usually used.

In the next simulation, it was observed that at the wavelength of 633 nm, Au, Cu, and Ag have the highest electric field enhancement. When using a Cu tip or substrate, it was observed that the use of Au next to it increases, and the use of Ag decreases, the enhancement of the electric field. When using an Ag tip or substrate, the use of Au or Cu, along with it, increases the enhancement of the electric field. It is more economical to use a thin layer of Au as a coating on a tip or a substrate made of Cu or Ag instead of using a tip and a substrate that is completely made of Au. In addition, Au and Cu coatings for Ag reduce corrosion against air.

Au coating for Cu reduces the chemical reaction when using it. Then, the effect of Au coating on the Cu tip and substrate and the effect of Au coating and Cu on the Ag tip and substrate were investigated at the wavelength of 633 nm. It was observed that the use of Au coating for Ag has a greater effect on increasing the enhancement than the cases of Au coating for Cu and Cu coating for Ag. However, the Au coating next to the Cu substrate creates a greater electric field enhancement.

Further, it was observed that the use of the same coating for the tip and the substrate is not very important. However, the same thickness of the coating on the tip provides higher enhancement than the coating on the substrate. The reason is the accumulation of more charges in the sharp places and, as a result, the density of free electrons in these places. The glass was used instead of Cu to investigate the effect of the material on the bottom layer of the substrate when using the coating on it. It was observed that the material of the bottom layer of the substrate has a great effect on electric field strengthening. It was also noted that different thicknesses of the lower layer of the substrate have a very different impact on the enhancement.

In the end, since metal surfaces are usually not biocompatible, five biocompatible materials were used as substrate coating. Using Au tip and Au substrate, different thicknesses were investigated. It was observed that muscovite mica, polystyrene, PVP, polyethylene, and PNIPAM create higher enhancement.

## References

- [1] Y. Cao, M. Sun, *Rev. Phys.* **8**, 100067 (2022).
- [2] C.V. Raman, K.S. Krishnan, *Nature* **121**, 501 (1928).
- [3] H. Khoshroo, H. Khadem, M. Bahreini, S. Tavassoli, J. Hadian, *Appl. Opt.* **54**, 9533 (2015).
- [4] M. Fleischmann, P.J. Hendra, A.J. McQuillan, *Chem. Phys. Lett.* **26**, 163 (1974).
- [5] S. Schlücker, *Angew. Chem. Int. Ed.* **53**, 4756 (2014).
- [6] Z. Zhang, S. Sheng, R. Wang, M. Sun, *Anal. Chem.* **88**, 9328 (2016).
- [7] J. Wessel, *J. Opt. Soc. Am. B* **2**, 1538 (1985).
- [8] P. Verma, *Chem. Rev.* **117**, 6447 (2017).
- [9] J. Dong, W. Gao, Q. Han, Y. Wang, J. Qi, X. Yan, M. Sun, *Rev. Phys.* **4**, 100026 (2019).
- [10] J. Ma, Y. Cheng, M. Sun, *Nanoscale* **13**, 10712 (2021).

- [11] Z. Zhang, P. Xu, X. Yang, W. Liang, M. Sun, *J. Photochem. Photobiol. C* **27**, 100 (2016).
- [12] J. Ma, J. Song, Y. Cheng, M. Sun, *J. Raman Spectrosc.* **52**, 1685 (2021).
- [13] S. Hagness, S. Ho, A. Taflove, in: *Computational Electromagnetics and Its Applications*, Eds. T.G. Campbell, R.A. Nicolaides, M.D. Salas, Springer, Dordrecht (Netherlands) 1997, p. 229.
- [14] B.T. Draine, P.J. Flatau, *J. Opt. Soc. Am. A* **11**, 1491 (1994).
- [15] D.B. Davidson, *Computational Electromagnetics for RF and Microwave Engineering*, Cambridge University Press, Cambridge 2010.
- [16] J.M. Jarem, P.P. Banerjee, *Computational Methods for Electromagnetic and Optical Systems*, CRC Press, 2016.
- [17] B. Engquist, A. Majda, *Proc. Natl. Acad. Sci.* **74**, 1765 (1977).
- [18] J.D. Jackson, *Classical Electrodynamics*, John Wiley & Sons, 2021.
- [19] Z. Yang, J. Aizpurua, H. Xu, *J. Raman Spectrosc.* **40**, 1343 (2009).
- [20] J. Stadler, B. Oswald, T. Schmid, R. Zenobi, *J. Raman Spectrosc.* **44**, 227 (2013).
- [21] N. Kazemi-Zanjani, S. Vedraïne, F. Lagugné-Labarthet, *Opt. Express* **21**, 25271 (2013).
- [22] L. Meng, T. Huang, X. Wang, S. Chen, Z. Yang, B. Ren, *Opt. Express* **23**, 13804 (2015).
- [23] M.K. Jahromi, R. Ghayour, Z. Adelpour, *Opt. Quant. Electron.* **53**, 385 (2021).
- [24] X. You, C.B. Casper, E.E. Lentz, D.A. Erie, J.M. Atkin, *ChemPhysChem* **21**, 188 (2020).
- [25] M. Bahreini, A. Hosseinzadegan, A. Rashidi, S.R. Miri, H.R. Mirzaei, P. Hajian, *Talanta* **204**, 826 (2019).
- [26] H. Chen, L. Yuan, W. Song, Z. Wu, D. Li, *Prog. Polym. Sci.* **33**, 1059 (2008).
- [27] J. Schubert, M. Chanana, *Curr. Med. Chem.* **25**, 4553 (2018).
- [28] J.D. Jackson, R.D. Fox, *Classical Electrodynamics*, John Wiley & Sons, 1999.
- [29] L. Li, K. Liu, B. Suen, Q. Liu, A. King, F.E. Talke, *Tribol. Lett.* **66**, 26 (2018).
- [30] S.A. Maier, *Plasmonics: Fundamentals and Applications*, Springer, 2007.
- [31] B. Sharma, R.R. Frontiera, A.-I. Henry, E. Ringe, R.P. Van Duyne, *Mater. Today* **15**, 16 (2012).
- [32] S. Kim, J. Jin, Y.-J. Kim, I.-Y. Park, Y. Kim, S.-W. Kim, *Nature* **453**, 757 (2008).
- [33] N. Anderson, A. Hartschuh, L. Novotny, *Mater. Today* **8**, 50 (2005).
- [34] T.-X. Huang, S.-C. Huang, M.-H. Li, Z.-C. Zeng, X. Wang, B. Ren, *Anal. Bioanal. Chem.* **407**, 8177 (2015).
- [35] Y. Liu, X. Li, H. Wu, Z. Zeng, D. Zhang, P. Wang, L. Zhang Y. Fang, *Plasmonics* **12**, 1861 (2017).
- [36] Y. Saito, M. Motohashi, N. Hayazawa, M. Iyoki, S. Kawata, *Appl. Phys. Lett.* **88**, 143109 (2006).
- [37] S. Seweryn, K. Skirlińska-Nosek, K. Sofińska, K. Szajna, J. Kobierski, K. Awiśuk, M. Szymoński, E. Lipiec, *Spectrochim. Acta A* **281**, 121595 (2022).
- [38] V. Giliberti, R. Polito, E. Ritter et al., *Nano Lett.* **19**, 3104 (2019).
- [39] M. Bahreini, *AIP Conf. Proc.* **1920**, 020013 (2018).
- [40] M. Bahreini, A. Noori, S.H. Aref, *J. Res. Many-body Syst.* **12**, 37 (2022).
- [41] X. Tan, Z. Wang, J. Yang, C. Song, R. Zhang, Y. Cui, *Nanotechnology* **20**, 445102 (2009).